Supporting Materials

A bifunctional cationic metal-organic framework based on nonanuclear copper(II) cluster for high dichromate and chromate trapping and highly efficient photocatalytic degradation of organic dyes under visible light irradiation

Tian-Rui Zheng, Lin-Lu Qian, Min Li, Zhi-Xiang Wang, Ke Li, Ya-Qian Zhang, Bao-Long Li* and Bing Wu
State and Local Joint Engineering Laboratory for Functional Polymeric Materials, College of Chemistry, Chemical Engineering and Materials Science, Soochow University, Suzhou 215123, PR China.

Experimental

Anion Exchange Studies

(1) Molar ratio 1:1 (1-NO_3-OH to 20 ppm $Cr_2O_7^{2-}$ or CrO_4^{2-})

1-NO_3-OH (3.4 mg, 0.00139 mmol) was immersed in a 15.0 mL 20ppm $Cr_2O_7^{2-}$ or **1-NO_3-OH** (6.8 mg, 0.00277 mmol) was immersed in a 16.0 mL CrO_4^{2-} aqueous solution and the mixture was mildly shaken at room temperature. The anion exchange process was monitored by liquid UV-vis spectroscopy based on typical absorption of $Cr_2O_7^{2-}$ at 257 nm or CrO_4^{2-} at 372 nm. 0.10 mL $Cr_2O_7^{2-}$ or CrO_4^{2-} aqueous solution was pipetted at different time interval to measure the UV-vis adsorption intensity.

(2) Selective capture of $Cr_2O_7^{2-}$

1-NO_3-OH (40 mg, 0.0163 mmol) was immersed in a 6.5 mL aqueous solution containing 2.5×10^{-3} mol/L $Cr_2O_7^{2-}$ and 2.5×10^{-2} mol/L ClO_4^-, 2.5×10^{-3} mol/L $Cr_2O_7^{2-}$ and 2.5×10^{-2} mol/L NO_3^-, or 2.5×10^{-3} mol/L $Cr_2O_7^{2-}$ and 2.5×10^{-2} mol/L Cl^-, or 2.5×10^{-3} mol/L $Cr_2O_7^{2-}$ and 2.5×10^{-2} mol/L BF_4^-, or 2.5×10^{-3} mol/L $Cr_2O_7^{2-}$ and 1.25×10^{-2} mol/L SO_4^{2-}, respectively. The mixture was mildly shaken at room temperature for 24 h. The resultant solids were used for IR measurement. The resultant solutions were all monitored by UV–vis absorbance measurement.

(3) Selective capture of CrO_4^{2-}

1-NO_3-OH (40 mg, 0.0163 mmol) was immersed in a 6.5 mL aqueous solution containing 2.5×10^{-3} mol/L CrO_4^{2-} and 2.5×10^{-2} mol/L ClO_4^-, 2.5×10^{-3} mol/L CrO_4^{2-} and 2.5×10^{-2} mol/L NO_3^-, or 2.5×10^{-3} mol/L CrO_4^{2-} and 2.5×10^{-2} mol/L Cl^-, or 2.5×10^{-3} mol/L CrO_4^{2-} and 2.5×10^{-2} mol/L BF_4^-, or 2.5×10^{-3} mol/L CrO_4^{2-} and 1.25×10^{-2} mol/L SO_4^{2-}, respectively. The mixture was mildly shaken at room

temperature for 24 h. The resultant solids were used for IR measurement. The resultant solutions were all monitored by UV–vis absorbance measurement.

(4) Release and cycle experiment

The release experiment was carried out right after the completion of an ion-exchange process of $Cr_2O_7^{2-}$ or CrO_4^{2-} at molar ratio 1:1 (**1-NO$_3$-OH** to 2.5×10^{-3} mol/L $Cr_2O_7^{2-}$ or CrO_4^{2-}. The **1-Cr$_2$O$_7$** or **1-CrO$_4$** was filtered and washed with water several times before release operation. The **1-Cr$_2$O$_7$** or **1-CrO$_4$** was immersed in a 6.5 mL 0.50 mol/L NO_3^- aqueous solution (200-fold molar excess) and the mixture was mildly shaken at room temperature for 48 h. The cycle experiments were done by performing ion-exchange, release, and filtering in turn for 5 cycles. The measurements were performed after completion of ion-exchange and release. The processes were all monitored by UV–vis absorbance measurement.

Table S1. Crystallographic data for **1-NO$_3$-OH·20H$_2$O**.

Formula	$C_{72}H_{84}Cl_2Cu_9N_{32}O_{24}$
Fw	2424.47
T/K	293(2)
Crystal system	hexagonal
Space group	$P6_3/m$
a/Å	18.438(4)
b/Å	18.438(4)
c/Å	18.792(4)
α (°)	90
β (°)	90
γ (°)	120
V /Å^3	5532(2)
F(000)	2454
Z	2
ρ_{calcd} (g cm^{-3})	1.455
μ(mm^{-1})	1.817
Reflections collected	12809
Unique reflections	3346 (R(int) = 0.0468)
Parameter	253
Goodness of fit	1.072
R_1 [I > 2σ(I)]	0.0475
wR_2 (all data)	0.1205

Table S2 Selected bond lengths and angles for **1-NO$_3$-OH·20H$_2$O** (Å and °).

Cu1-O1	1.960(2)	Cu1-O2	1.964(2)
Cu1-N1	2.036(3)	Cu1-N4B	1.974(3)
Cu1-Cl1	2.7046(9)	Cu2-O1	1.964(2)
Cu2-O3	2.214(4)	Cu2-O5C	1.960(4)
Cu2-N2	2.029(3)	Cu2-N2A	2.029(3)
O1-Cu1-O2	82.25(11)	O1-Cu1-N1	86.65(12)
O1-Cu1-N4B	168.22(13)	O2-Cu1-N1	167.20(12)
O2-Cu1-N4B	95.19(12)	N1-Cu1-N4B	94.40(13)
O1-Cu1-Cl1	98.22(10)	O2-Cu1-Cl1	95.03(10)
N1-Cu1-Cl1	92.83(9)	N4B-Cu1-Cl1	93.45(10)
O1-Cu2-O3	102.56(16)	O1-Cu2-O5C	177.98(17)
O1-Cu2-N2	85.68(9)	O1-Cu2-N2A	85.67(9)
O3-Cu2-O5C	79.46(19)	O3-Cu2-N2	95.24(9)
O3-Cu2-N2A	95.24(9)	O5C-Cu2-N2	94.17(9)
O5C-Cu2-N2A	94.17(9)	N2-Cu2-N2A	167.64(18)

Symmetry transformations used to generate equivalent atoms: A +X, +Y, 1/2-Z; B 1-Y, +X-Y, +Z; C 1-Y, 1+X-Y, +Z for **1-NO_3-OH·20H_2O.**

Table S3 Adsorption capacities for chromate or dichromate on various porous materials.

Cationic MOF	***Maximum capacity***		***Reference***
	CrO_4^{2-}	**$Cr_2O_7^{2-}$**	
A 2D Ag based-MOF (**SLUG-21**)	60 mg/g or 0.41 mol/mol		S1
A 3D Dy-MOF (**1-ClO_4**)	62.88 mg/g or 0.85 mol/mol		S2
$Zn_{0.5}Co_{0.5}$SLUG-35	68.5 mg/g or 0.43 mol/mol		S3
A 3D Ag-based MOF		0.73 mol/mol	S4
FIR-53		74.2 mg/g	S5
FIR-54		103.1 mg/g	
A post-synthesized Zr-MOF (**ZJU-101**)		245 mg/g	S6.
A 3D Ni based MOF		166 mg/g	S7
A 3D MOF tetranuclear copper(II) cluster (**1-Br**)		128 mg/g, 0.84 mol/mol	S8

A 3D Ag based MOF		207mg/g	S9
$\{[Ag(L_1)_2](BF_4)\}_n$		81.9 mg/g	S10
A 2D Cd based MOF		116.6 mg/g	S11
A Zr-MOF (**MOR-2** via power X-ray crystallography)	118.3 mg/g	193.7 mg/g	S12
MOR-2-HA	109 mg/g	162.8 mg/g	
A 2D MOF based on nonanuclear copper(II) cluster (**1-NO_3-OH**)	89.5 mg/g, 1.896 mol/mol	154.8 mg/g, 1.762 mol/mol	This work
Other types Adsorbents	***Maximum capacities for Cr(VI) (mg/g)***		**Reference**
Amino starch	12.12 mg/g		S13
β-CD and quaternary ammonium groups modified cellulose	61.05 mg/g		S14
Hexadecylpyridinium bromide modified natural zeolites	14.31 mg/g		S15
Modified magnetic chitosan chelating resin	58.48 mg/g		S16
Amino-functionalized titanate nanotubes	153.85 mg/g		S17

Reference

S1 H. Fei, M. R. Bresler and S. R. J. Oliver, *J. Am. Chem. Soc.*, 2011, **133**, 11110.

S2 P. F. Shi, B. Zhao, G. Xiong, Y. L. Hou and P. Cheng, *Chem. Commun.*, 2012, **48**, 8231.

S3 H. Fei, C. S. Han, J. C. Robins and S. R. J. Oliver, *Chem. Mater.*, 2013, **25**, 647.

S4 X. X. Li, H. Y. Xu, F. Z. Kong and R. H. Wang, *Angew. Chem. Int. Ed.*, 2013, **52**, 13769.

S5 H. R. Fu, Z. X. Xu and J. Zhang, *Chem. Mater.*, 2015, **27**, 205.

S6 Q. Zhang, J. C. Yu, J. F. Cai, L. Zhang, Y. J. Cui, Y. Yang, B. L. Chen and G. D. Qian, *Chem. Commun.*, 2015, **51**, 14732.

S7 A. V. Desai, B. Manna, A. Karmakar, A. Sahu and S. K. Ghosh, *Angew. Chem. Int. Ed*., 2016, **55**, 7811.

S8 X. X. Lv, L. L. Shi, K. Li, B. L. Li, H. Y. Li, *Chem. Commun*., 2017, **53**, 1860.

S9 C. P. Li, H. Zhou, S. Wang, J. Chen, Z. L. Wang, M. Du, *Chem. Commun*., 2017, **53**, 9206.

S10 K. Nath, K. Maity, K. Biragha, *Cryst. Growth Des.*, 2017, **17**, 4437.

S11 H. R. Fu, Y. Zhao, Z. Zhou, X. G. Yang, L. F. Ma, *Dalton Trans*., 2018, **47**, 3725.

S12 S. Rapti, D. Sarma, S. A. Diamantis, E. Skliri, G. S. Armatas, A. C. Tsipis, Y. S. Hassan, M. Alkordi, C. D. Malliakas, M. G. Kanatzidis, T. Lazarides, J. C. Plakatouras, *J. Mater. Chem. A,* 2017, **5**, 14707.

S13 A. Dong, J. Xie, W. Wang, L. Yu, Q. Liu and Y. Yin, *J. Hazard. Mater.*, 2010, **181**, 448.

S14 Y. Zhou, Q. Jin, T. Zhu and Y. Akama, *J. Hazard. Mater.*, 2011, **187**, 303.

S15 Y. Zeng, H. Woo, G. Lee and J. Park, *Microporous Mesoporous Mater.*, 2010, **130**, 83.

S16 Y. G. Abou El-Reash, M. Otto, I. M. Kenawy and A. M. Ouf, *Int. J. Biol. Macromol.*, 2011, **49**, 513.

S17 L. Wang, W. Liu, T. Wang and J. Ni, *Chem. Eng. J.*, 2013, **225**, 153.

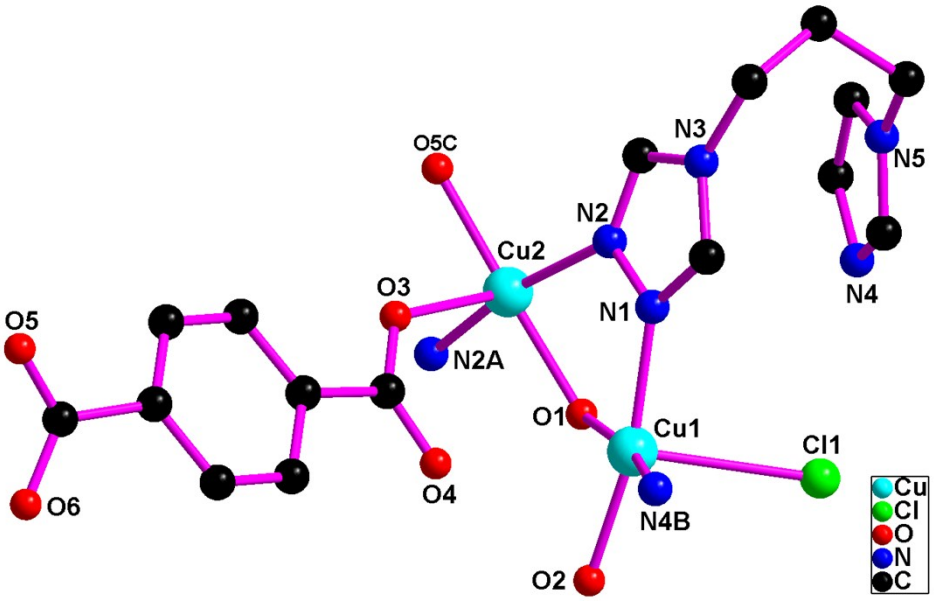

Fig. S1 The coordination environment of the Cu(II) atoms in **1-NO_3-OH·20H_2O**.

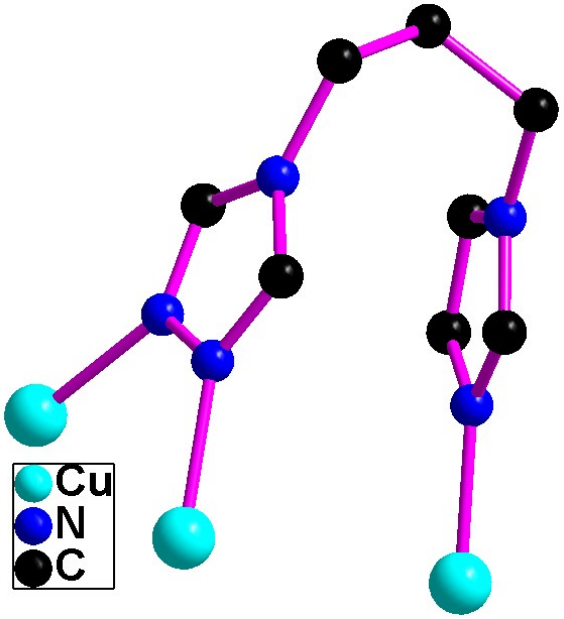

Fig. S2 The coordination mode of itp ligand in **1-NO_3-OH·20H_2O**.

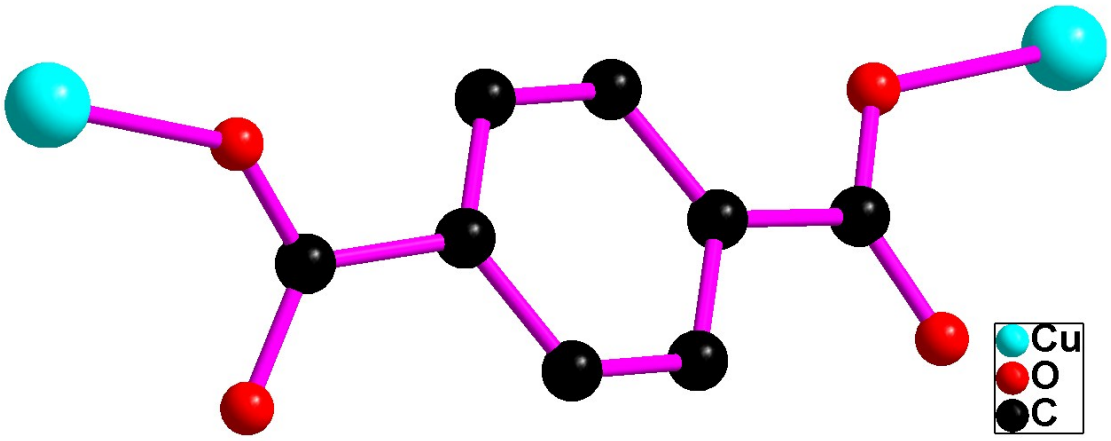

Fig. S3 The coordination mode of 1,4-bdc ligand in **1-NO_3-OH·20H_2O**.

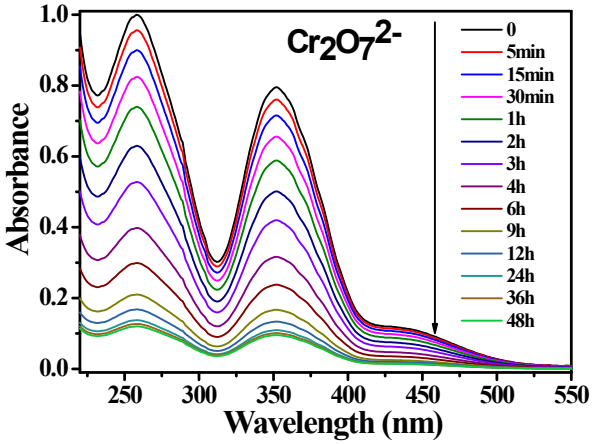

Fig. S4 UV/Vis spectra of $Cr_2O_7^{2-}$ aqueous solution during exchange with equimolar **1-NO_3-OH** and 20 ppm $Cr_2O_7^{2-}$ aqueous solution.

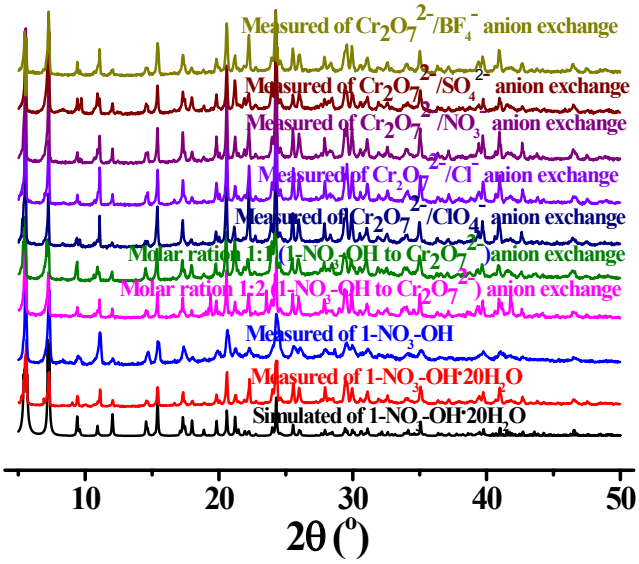

Fig. S5 PXRD patterns for simulated and measured of **1-NO_3-OH·20H_2O**, measured of **1-NO_3-OH**, molar ratio 1:2 and 1:1 (**1-NO_3-OH** to **$Cr_2O_7^{2-}$**) anion exchange, and molar ratio 1:1 (**1-NO_3-OH** to **$Cr_2O_7^{2-}$**) in the presence of interfere anions.

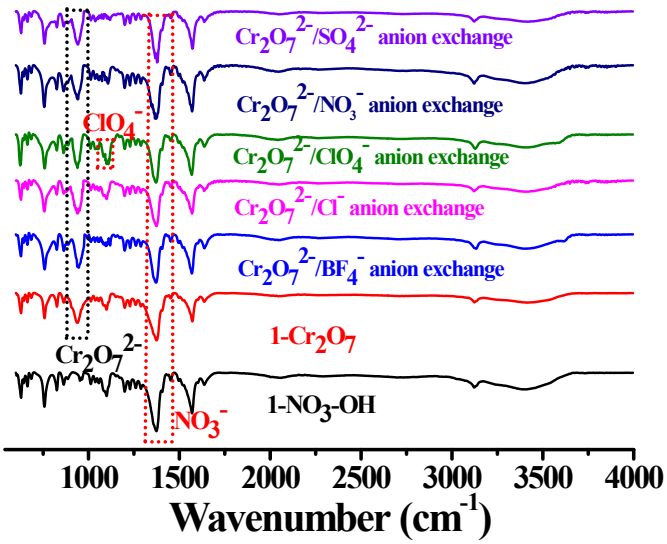

Fig. S6 IR spectra for **1-NO_3-OH**, **1-Cr_2O_7** and **1-NO_3-OH** immersed in the mixed aqueous solution during anion exchange.

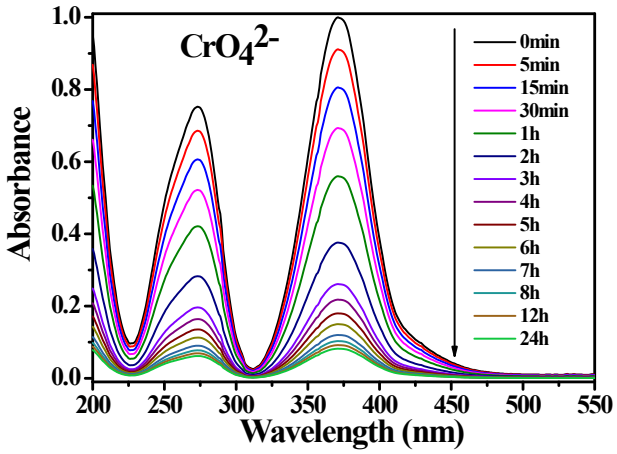

Fig. S7 UV/Vis spectra of CrO_4^{2-} aqueous solution during exchange with equimolar **1-NO_3-OH** and 20 ppm CrO_4^{2-} aqueous solution.

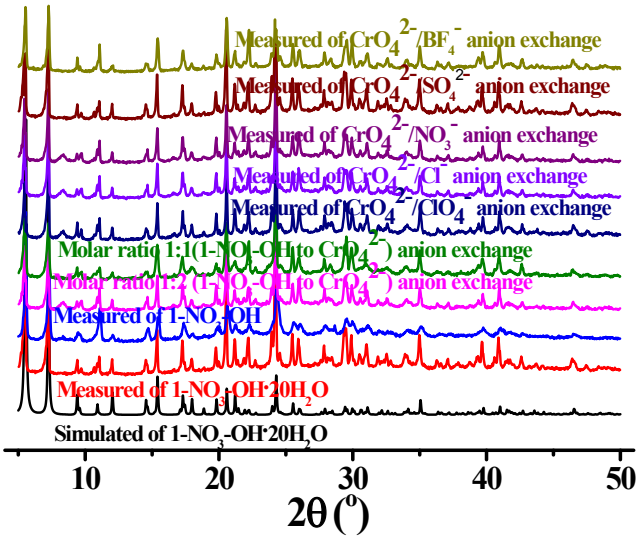

Fig. S8 PXRD patterns for simulated and measured of **1-NO_3-OH·20H_2O**, measured of **1-NO_3-OH**, molar ratio 1:2 and 1:1 (**1-NO_3-OH** to **CrO_4^{2-}**) anion exchange, and molar ratio 1:1 (**1-NO_3-OH** to **CrO_4^{2-}**) in the presence of interfere anions.

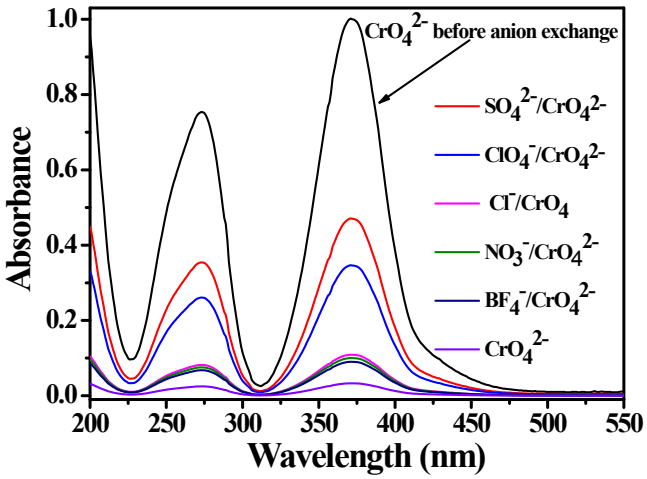

Fig. S9 UV-vis spectra of the mixed aqueous solution during anion exchange.

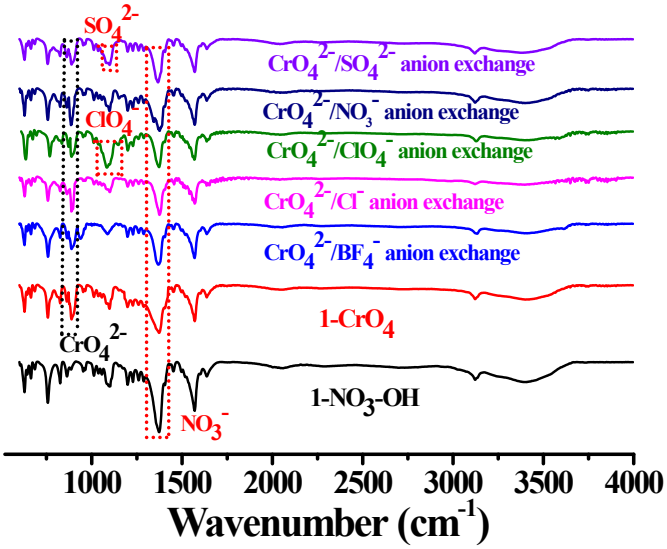

Fig. S10 IR spectra for **1-NO_3-OH, 1-CrO_7** and **1-NO_3-OH** immersed in the mixed aqueous solution during anion exchange.

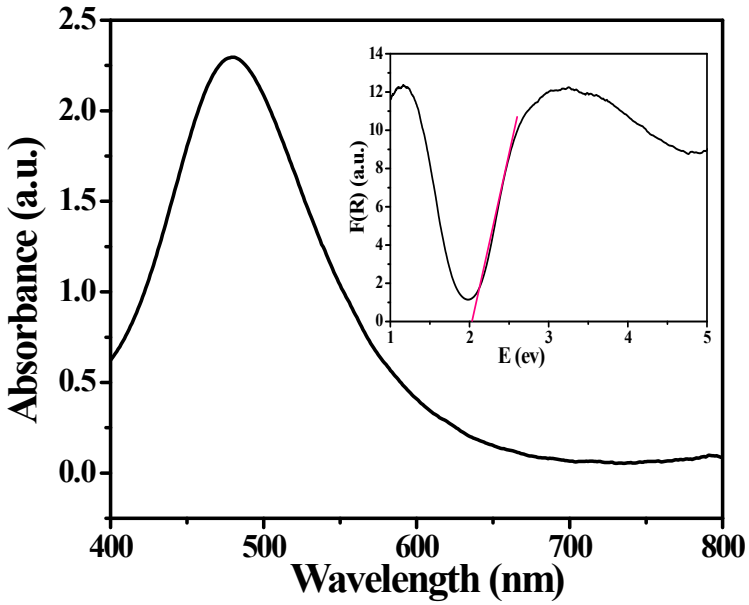

Fig. S11 The UV-visible absorption spectra of the photocatalyst **1-NO_3-OH·20H_2O**.

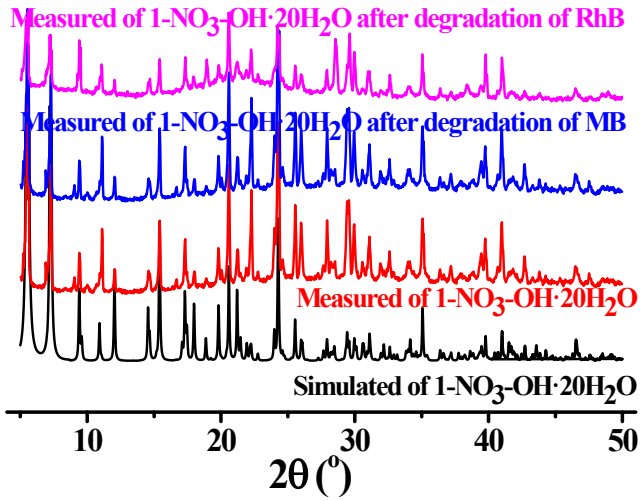

Fig. S12 PXRD patterns for simulated and measured of **1-NO_3-OH·20H_2O**, and measured of **1-NO_3-OH·20H_2O** after photocatalytic degradation of MB or RhB.

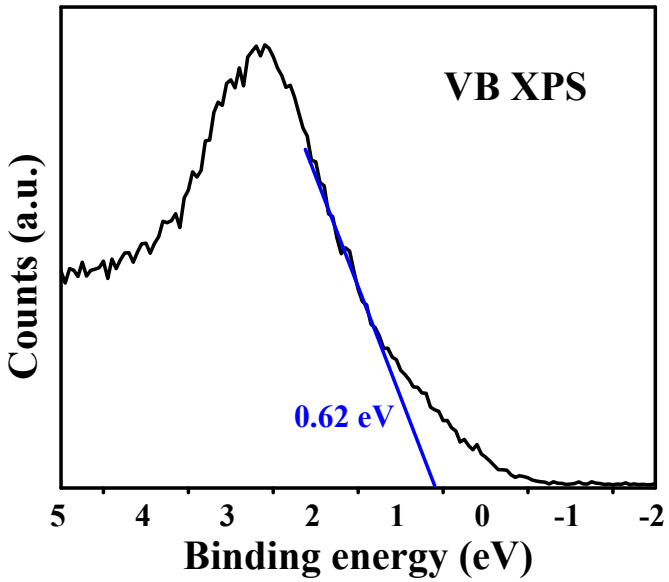

Fig. S13 Valence band XPS result of the photocatalyst **1-NO_3-OH·20H_2O**.

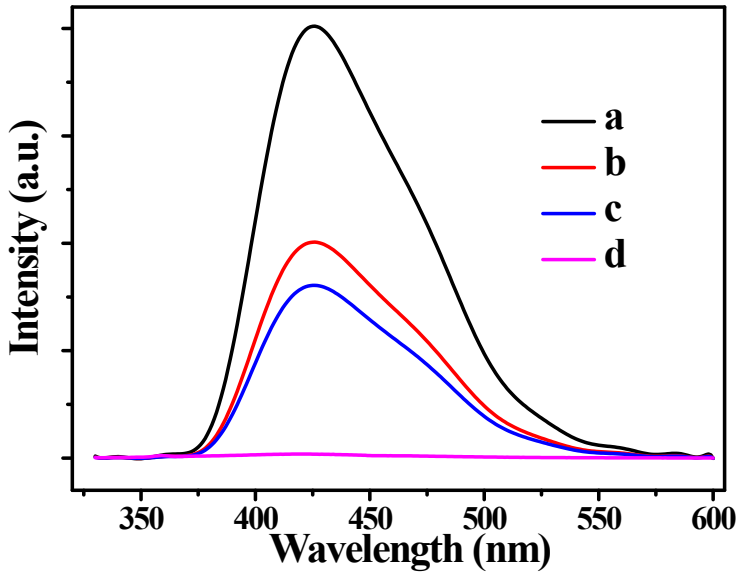

Fig. S14 The photoluminescence spectra of TAOH formed by the reaction of TA with •OH radicals generated from different photocatalytic systems under visible light for 10 min. (a) in the presence of **1-NO_3-OH·20H_2O** and H_2O_2; (b) only **1-NO_3-OH·20H_2O**; (c) only H_2O_2; and (d) without the photocatalyst and H_2O_2.